FINNISH METEOROLOGICAL INSTITUTE

AMS 35TH CONFERENCE ON RADAR METEOROLOGY PITTSBURGH, PA, USA_ Sep2011

Nevvonen Ljubov, Saltikoff Elena

First experiences of operational use of a dual-polarisation weather radar in Finland

1. Finnish Weather Radar network

The FMI radar network consists of 8 C-band Doppler radars. The maximum coverage range of 250 km is plotted as a circle around each side. Vantaa radar (upgraded 2009), used in the examples of this paper, is in middle of the south coast. Two other radars (upgraded 2009 and 2010), Anjalankoski east of Vantaa and Ikaalinen northwest of Vantaa (marked with triangles).

Our experience after a few months of usage is illustrated with three case studies in weather situations typical of the Finnish climate.

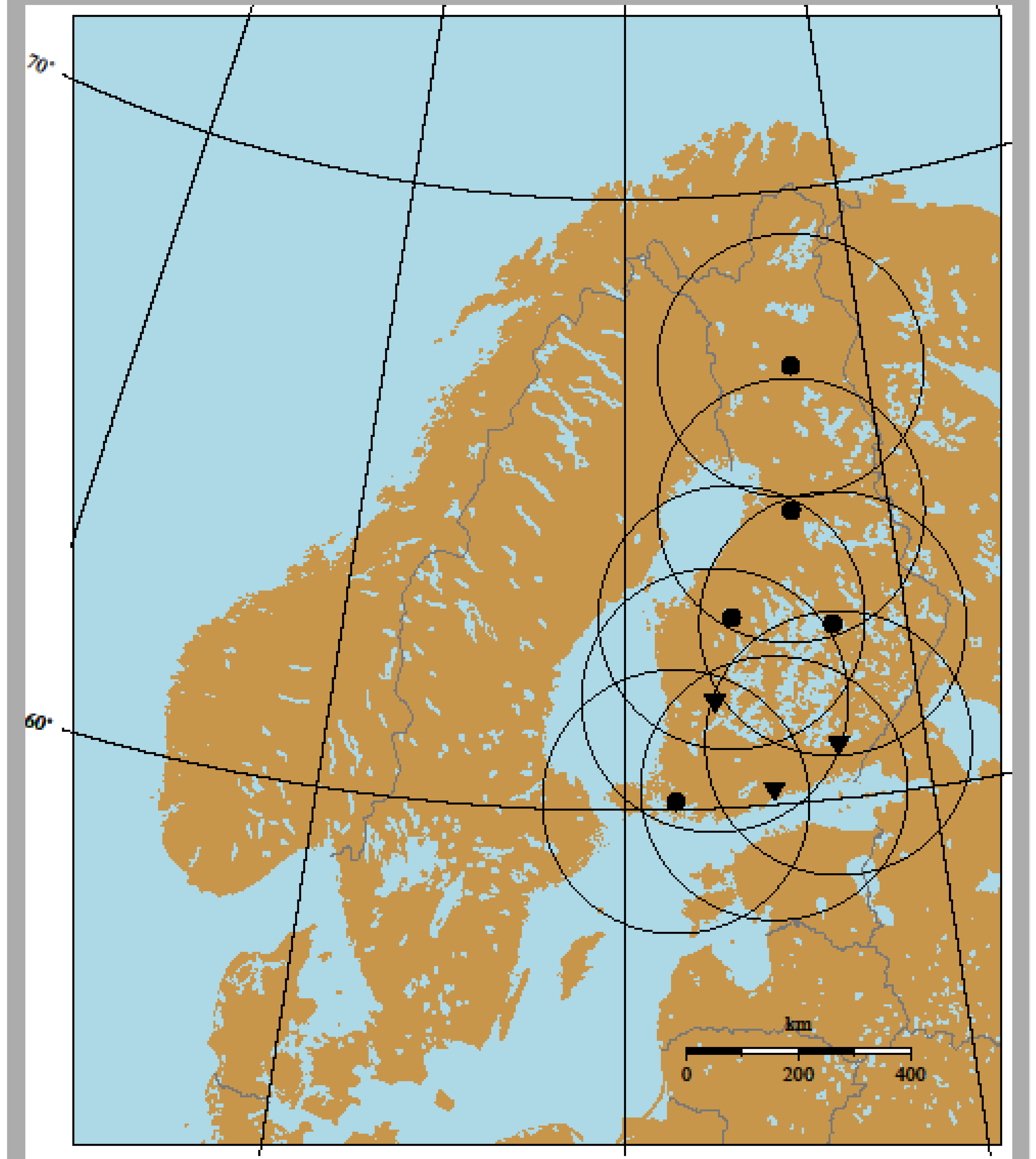

Fig. 1 FMI's radar network

2. The measurement schedule

- twelve PPI scans
- two RHI scans
- different PRFs
- different pulse widths
- different processing modes
- STAR and LDR modes
- to be repeated at least oncle every 15 minutes

Within this 15 min period, the high elevation PPIs (Group C) and LDR measurement for research purposes (Group D) are repeated once, the low-level PPIs with high-quality wind data (Group B) - twice and the low- and middle level measurements with dual-polarisation mode (Group A) - three times.

Fig. 2 Elevation angles

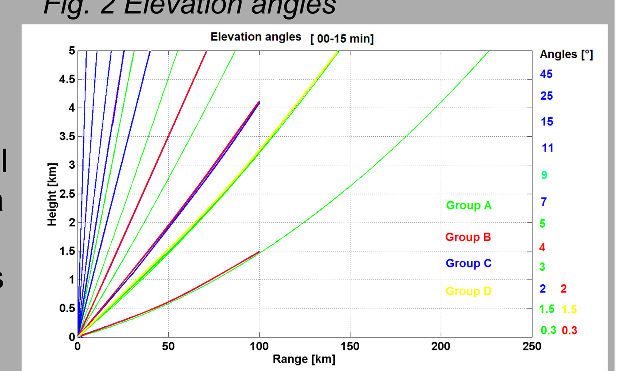

Table 1. Characteristics of the measurements

Time, min	0	01:54	03:54	5	07:12	08:07	08:43	10	12:15	13:13	14:13	15
TASKS	0	Group A	Group C	5	Group A	Group B	Group D	10	Group A	Group B	Group E	15
Scan mode	0	PPI Full	PPI Full	5	PPI Full	PPI Full	PPI Full	10	PPI Full	PPI Full	RHI	15
Azimuth, °	0	Full Circ.	Full Circ.	5	Full Circ.	Full Circ.	Full Circ.	10	Full Circ.	Full Circ.	0, 180	15
Elevation, °	0	0.3, 1.5	2, 7, 11	5	0.3, 1.5	0.3, 2, 4	1,5	10	0.3, 1.5	0.3, 2, 4	from 0.0	15
	0	3, 5, 9	15, 25, 45	5	3, 5, 9			10	3, 5, 9		to 60	15
Pulse, µs	0	Long 2	Short 1	5	Long 2	Short 1	Long 2	10	Long 2	Short 1	Long 2	15
Polarization	0	Dual H+V	Single H	5	Dual H+V	Single H	Single H	10	Dual H+V	Single H	Dual H+V	15
Data	0	Z,T,V,W,ZDR,	Z,T,V,W,SQI	5	Z,T,V,W,ZDR,	Z,T,V,W,SQI	Z,T,V,W,SQI,	10	Z,T,V,W,ZDR,	Z,T,V,W,SQI	Z,T,V,W,ZDR,	15
	0	RhoHV,PhiDP,		5	RhoHV,PhiDP,		LDRh	10	RhoHV,PhiDP,		RhoHV,PhiDP,	15
	0	SQI,KDP,HCL		5	SQI,KDP,HCL			10	SQI,KDP,HCL		SQI,KDP,HCL	15
Range,km	0	249,9	99,9	5	249,9	99,9	249,9	10	249,9	99,9	150	15
PRF, Hz	0	570	1400/ 1050	5	570	1400/ 1050	570	10	570	1400/ 1050	570	15
Nyquist, m/s	0	7,6	56	5	7,6	56	7,6	10	7,6	56	7,6	15
Processing	0	PPP	RPHASE	5	PPP	RPHASE	PPP	10	PPP	RPHASE	PPP	15
Mode	0	STAR	LDR	5	STAR	LDR	LDR	10	STAR	LDR	STAR	15
min / group	0	01:54	02:00	5	02:12	00:55	00:36	10	02:15	00:58	01:00	15

3. Applications: appraising the benefits from the new data retrieved in different weather situations

A case of stratiform precipitation (Oct 3, 2009)

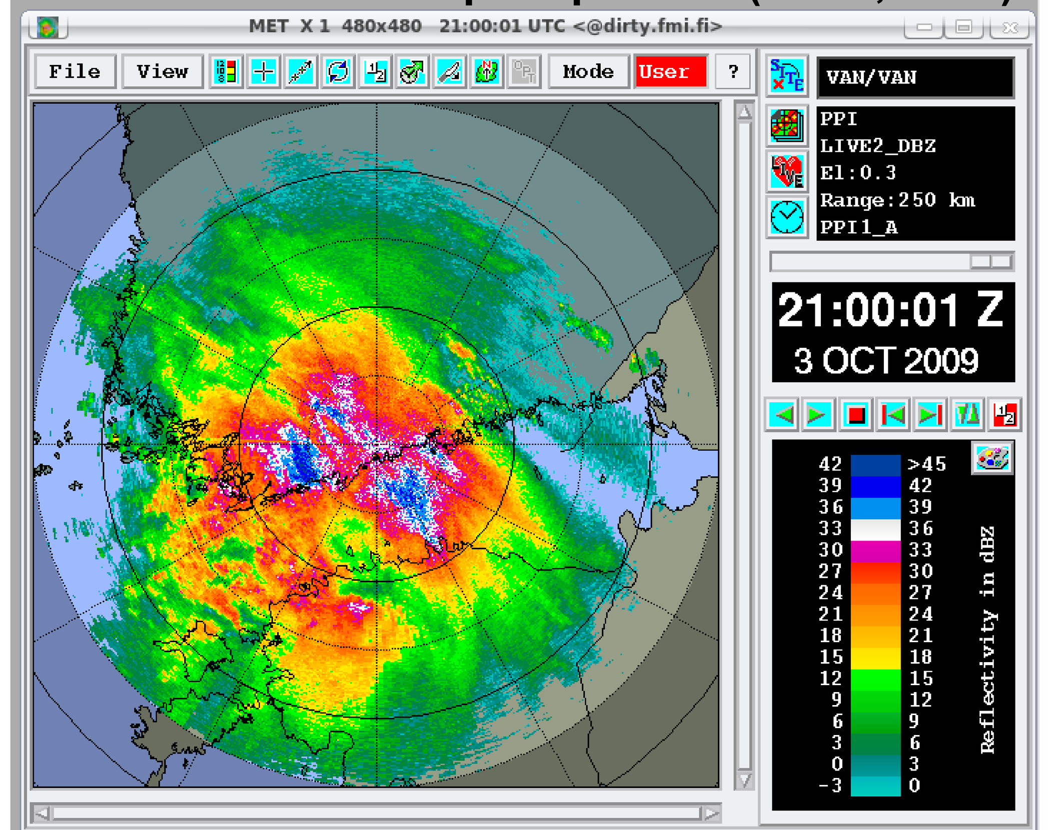

Fig.3 Vantaa radar images October 3, 2009 at 21 UTC : PPI at 0.3 degrees elevation reflectivity dBZ. The range from the radar depicted by rings spaced every 50 km.

This is a case of widespread precipitation, related to a warm front moving over Southern Finland from west to east on 3rd Oct 2009. Rain was observed at ground level, but the melting layer was low, so that most of the measurements were made in snow.

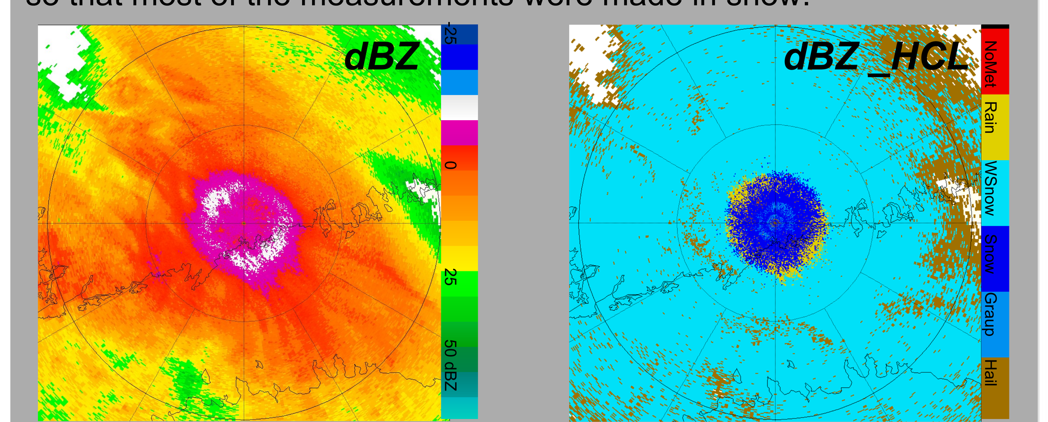

Fig.3a PPI at 1.5 degrees elevation on the left, hydrometer classification on the right.

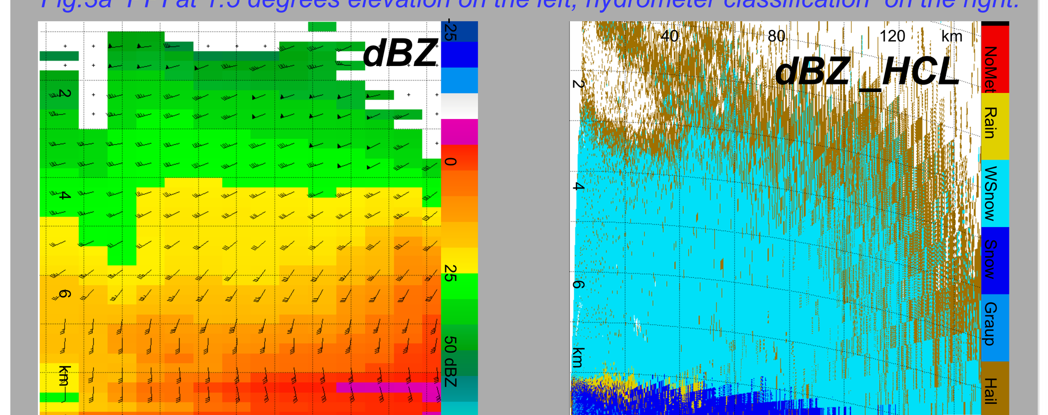

Fig.3b THVVP wind and reflectivity profile every 15 minutes 17:30-20:45 (left) and hydrometeor classification HCL RHI to south of radar (right).

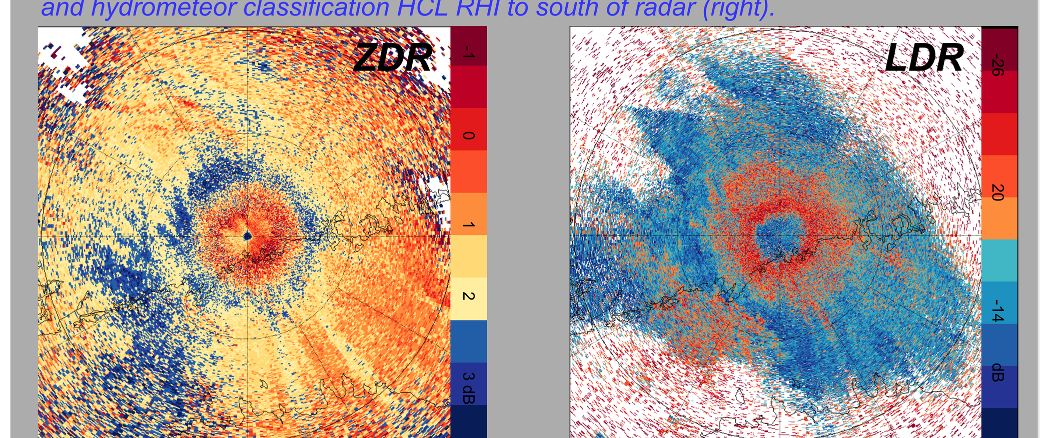

Fig.3c PPI at 0.3 degrees elevation: differential reflectivity ZDR on the left, linear depolarisation ratio LDR on the right.

- At 21:00 UTC, when the surface front had reached the radar site, a very sharp melting layer is seen in the vertical reflectivity profile as well as in the RHI's (Fig.3b,right) .The bright band extends from 400 m to 1000 m with amplitude of 30 dBZ. Reflectivity peaks 40 dBZ at 800 m.
- In the melting layer RhoHV decreased to 0.8 (not shown) and ZDR increased up to1.6 dB (Fig.3c,left).
- In the hydrometeor classification based on these indicators (Figs. 3a and 3b, right panels), the shift from dry snow to wet snow is consistent with this melting layer signature. The bright band is more pronounced near the radar than further away. At a height of 800 metres the beam is full of melting snow, and above that, at a height of 1000 meters, it is full of dry snow.
- The areas of high LDR and low ZDR are sometimes, but not always, co-located (Fig.3c).
- The wind profiles (Fig. 3b, right) show winds veering and increasing with height, consistent with warm advection and classification of the case as a warm front.

A cold front (September 4, 2009)

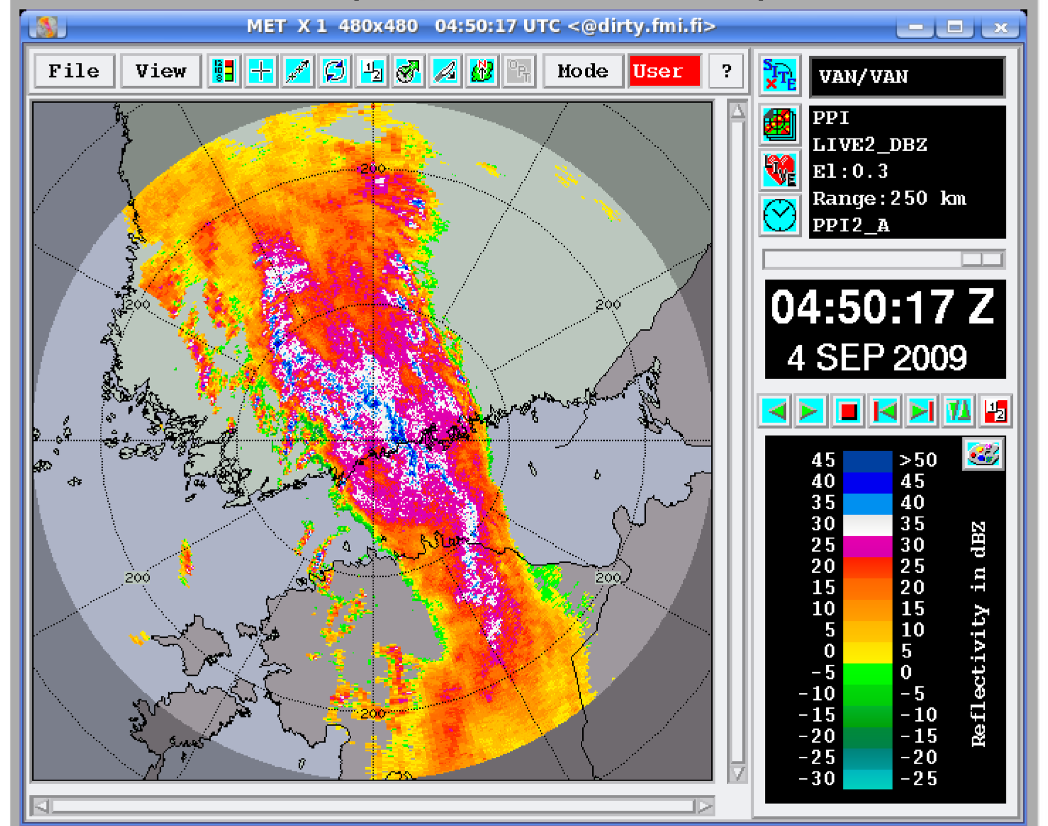

Fig.4 Vantaa radar images September 4, 2009 at 4:50 UTC: PPI at 0.3 degrees elevation reflectivity dBZ.The range from the radar depicted by rings spaced every 50 km.

A cold front passed over the radar with reflectivity up to 45 dBZ being observed within rain bands in the large scale precipitation area. The area itself was much longer than the 500 km coverage of the radar, but only 80- 100 km wide.

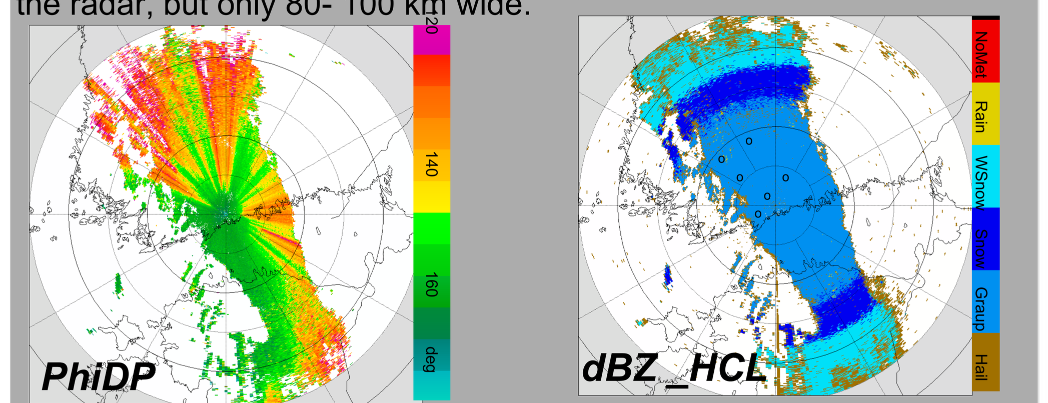

Fig.4a PPI at 0.3 degrees elevation: Differential phase PhiDP on the left , HCL on the right (locations of gauges used for comparison marked with circles).

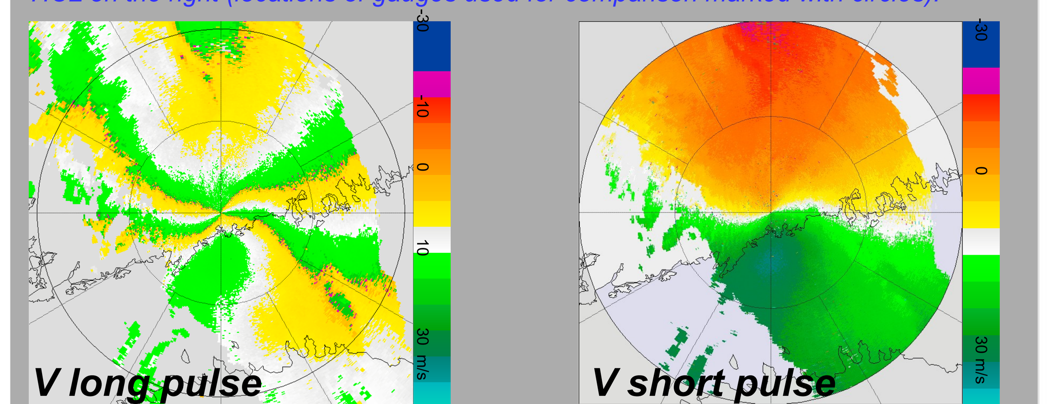

Fig.4b PPI at 0.3 degrees elevation: Doppler velocity from the long pulse on the left and Doppler velocity from the short-pulse dual-PRF measurement 2 min later on the right.

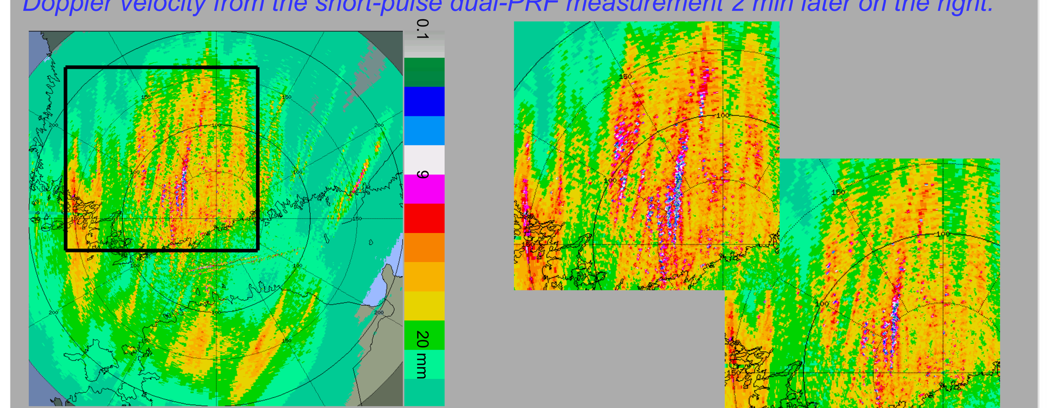

Fig.4c 24 h accumulated precipitation until 6 UTC: uncorrected on the left, corrected with dual-polarisation attenuation correction in the middle and corrected with reflectivity-based attenuation correction on the right. The zooming area marked in the first panel.

- Dual-polarisation parameters suggest the presence hail and graupel inside the embedded convective cores near the melting layer.
- PhiDP(Fig.4a, left) and ZDR (not shown) indicate attenuation in these cores. Dry hail would not affect PhiDP.
- Hydrometer classification (Fig.4a, right) shows rain in the middle of the image, melting snow at a distance of 150 km and dry snow at the edges.
- Velocities in the main task (A) are badly folded (Fig.4b, left); in the velocity task measurement 2 minutes later, random-phase unfolding reveals radial speeds up to 25 m/s (Fig.3b right).
- Fig. 3c shows the 24-hour accumulated precipitation first without any attenuation corrections, compared to images where the new dual-polarisation based correction (middle panel) and the conventional reflectivity-based correction (right panel) were used. The differences between the two correction methods are very small. The "fishbone" striped pattern is due to the motion of the strongest cells during the 5-minute intervals between volume scans.

A convective case (September 3, 2009)

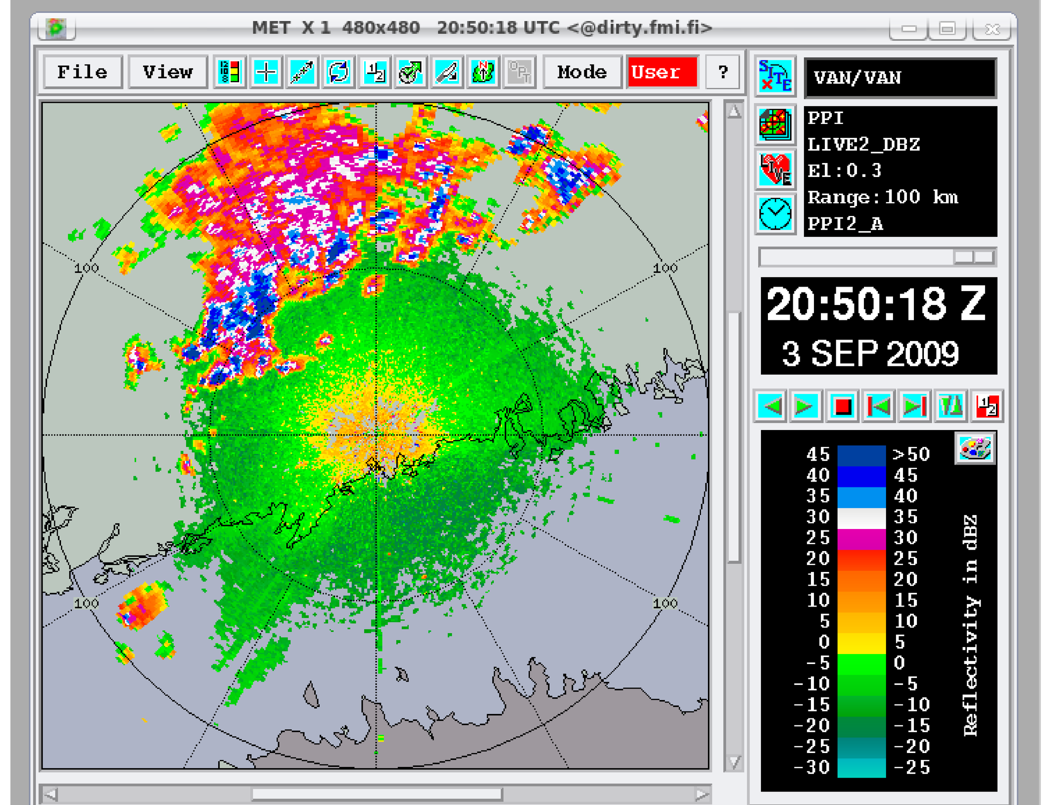

Fig.5 Vantaa radar images September 3, 2009 at 20:50 UTC: PPI at 0.3 degrees elevation reflectivity dBZ.The range from the radar depicted by rings spaced every 50 km.

Convective cells were observed north of the radar at a distance of 50-100 km, as seen in the reflectivity image (Fig.5). An area of clear air echoes (CAE) is seen out to 50 km from the radar in this image, but only out to 30 km in the random phase task (Fig. 5a, left).

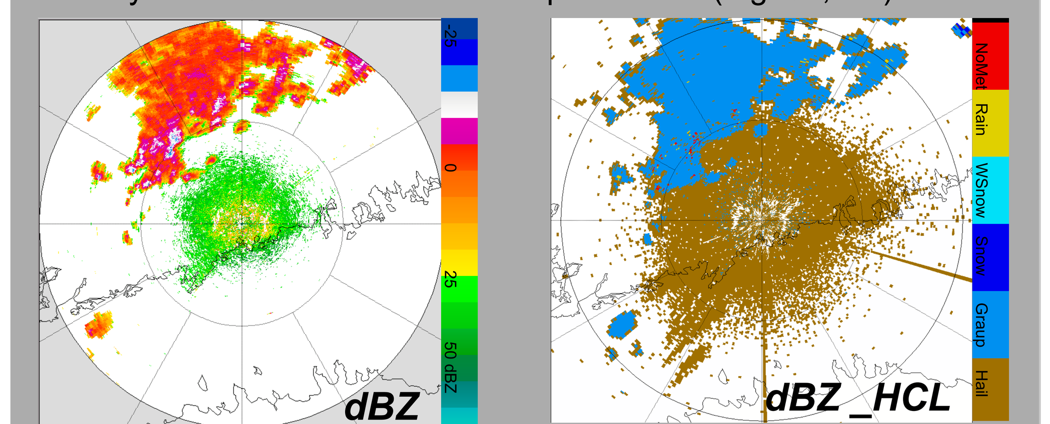

Fig.5a PPI at 0.3 degrees elevation: reflectivity dBZ (shot pulse) on the left, hydrometeorological classification on the right.

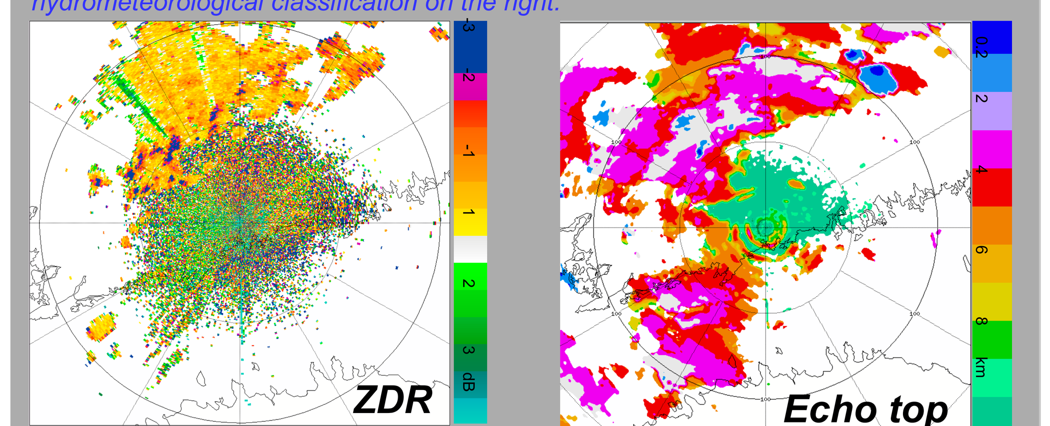

Fig.5b PPI at 0.3 degrees elevation differential reflectivity ZDR on the left, Echo tops with threshold –10 dBZ on the right.

- Hydroclass nicely separates the CAE from the rain. Interference from external microwave emitters is seen as two streaks towards South and southeast (Fig.5a, right).
- Even though it is not obvious in the reflectivity image, there is some attenuation towards the northwest, as can be seen as the sector of negative ZDR values in the ZDR image (Fig.5b, left).
- The Echo top image with a threshold of -10 dBZ (Fig.5b, right) shows the high anvils in convective clouds, and the low tops of the clear airechoes. This image contains radar-centred rings due to Insufficient resolution in elevation.

4.Discussion

The three cases show that dual-polarisation reveals properties of precipitation events not seen with conventional radar data.

The first case illustrates the challenge of precipitation type classification: even though all surface observations show rain, most of the radar measurements are made in snow, due to the measurement geometry and the spherical shape of the earth.

In the second case, it was possible to detect hail and graupel within the precipitation system. A short test of the attenuation scheme showed, on average, that the dual-polarisation (PhiDP)- based attenuation correction scheme performed as well as the conventional attenuation correction scheme.

In the third convective case, the echoes from non-precipitation targets are correctly identified, but at the moment there is no procedure to clean up the rainfall intensity images by removing such echoes.

References: Doviak R.J., D. Zrnic, 2006: Doppler Radar and Weather Observations: Second Edition. -- Dover Publications. ISBN: 0486450600. 562 pp. Fu, D., X. Guo, 2007: Numerical study on a severe downburst-producing thunderstorm on 23 August 2001 in Beijing -- Advances in Atmospheric Sciences **24**, 227 –238. Joe, P., P.T. May, 2003: Correction of Dual PRF Velocity Errors for Operational Doppler Weather Radars. -- J. Tech.., **20**, 429–442. Leskinen M, I. Markkula, J. Koistinen, P. Pylkkö, S. Ooperi, P. Siljamo, H. Ojanen, S. Raiskio, K. Tiilikkala, 2009: Pest insect immigration warning by an atmospheric dispersion model, weather radars and traps. (accepted, Journal of Applied Entomology). Vaisala 2009. RVP 8 Doppler signal processor user's manual. -- Vaisala, P.O. Box 26, FI-00421 Helsinki, Finland